Progress In Electromagnetics Research B, Vol. 97, 37–54, 2022

Electromagnetic Simulation for Robust Recognition Algorithm of Radar Target by Homing Missiles

Alaa G. A. Abd-Elfattah[1], Khalid F. A. Hussein[2, *], Asmaa E. Farahat[2], and Magdy A. Kotb[3]

Abstract—A novel signal processing scheme for identification of jet fighter targets by the onboard radar of active and hybrid homing missiles is proposed in the present work. For a specific target, the frequencies of the internal resonances of the cavity-backed apertures existing as the air-inlet pipes of the jet engine are used to construct an interior signature function for the proposed target identification scheme. For the purpose of quantitative description and assessment of the proposed scheme, electromagnetic simulation is used where the air-inlet pipe is modeled as an open-ended conducting cylinder with a number of radial conducting blades placed inside the cylindrical cavity near the open end. The transmitted radar pulse is formed by frequency chirping using linear frequency modulation (LFM) to include the frequencies in the band 1.0–2.0 GHz with high sweep resolution. The selected frequency band is wide enough to distinguish among various jet fighter targets. The CST® simulator is used to evaluate the radar cross section (RCS) of the open-ended pipe model with the internal blades due to an incident chirped pulsed plane wave as mentioned above over the frequency band 1.0–2.0 GHz. The proposed target identification algorithm is mathematically described and computationally applied to identify different targets with different dimensions of the jet engine pipe. The effect of the additive white Gaussian noise (AWGN) on the correctness of the target identification decision using the proposed scheme is investigated by calculating the false alarm rate (FAR) with varying the signal-to-noise ratio (SNR). The numerical examinations show that the proposed algorithm succeeds in taking the correct decision regarding the target identification with FAR $< 10\%$ for SNR ≥ 12 dB.

1. INTRODUCTION

Attacking jet fighters represent a grave danger to civilian facilities and individuals and may cause heavy losses in the military personnel and equipment if they are not confronted with a decisive response from the air defense system. Therefore, they should be targeted by defending missiles launched from sea, land, or air once they approach the national airspace. When the homing missile is launched towards the attacking jet fighter, it should start a mission of four tasks: (i) detection of the target, (ii) tracking the target motion, (iii) approaching the target, and finally, (iv) exploding at homing. Correct and fast target identification decision is necessary during these tasks; otherwise, the missile will fail to track, and the target will escape.

An example of a homing missile launched by a ship is presented in Figure 1(a). Cavity-backed apertures are encountered in the fighter aircrafts as air inlets and engine tubes; see, for example, Figure 1(b). These cavity-backed apertures contribute a great deal to the radar cross section (RCS) of attacking jet fighters. At the frequencies corresponding to the internal resonances of these cavities, the target RCS as a function of the frequency is characterized by very sharp maxima and minima that

Received 15 September 2022, Accepted 14 October 2022, Scheduled 26 October 2022
* Corresponding author: Khalid Fawzy Ahmed Hussein (fkhalid@eri.sci.eg).
[1] High Institute of Electronic Engineering, Belbis, Egypt. [2] Electronics Research Institute (ERI), Cairo 11843, Egypt. [3] Faculty of Electronic Engineering, Menoufia University, Menoufia, Egypt.

(a) (b)

Figure 1. (a) Missile launched by a ship to track an attacking fighter aircraft. (b) Example of fighter aircraft whose jet engine exhaust pipe has the common shape of a cylinder with circular open ends as air inlet and exhaust outlet.

is closely related to the dimension of the cavity and the aperture. Such resonances can be easily used to recognize the attacking target [1]. The pipes attached to the jet engines are used as air inlets and exhaust outlet; see Figure 1(b). These pipes are usually modeled as open-ended conducting cylindrical tubes of practical dimensions with radial conducting blades placed inside the cylindrical cavity [2–7].

A self-guided or passive homing missile has an infrared detector; see Figure 2(a). This missile detects the heat emitting from the exhaust of the aircraft jet engine via the head infrared detector relative to the cool environment of the sky or land. Radar-based homing missiles can be categorized into semi-active, active, and hybrid homing missiles. An active homing missile has microwave radar; see Figure 2(b). These types of missiles transmit the radar signal and receive the radar return (echo) and, then, perform signal processing for target identification. In semi-active homing missiles, a land, ocean, or airborne radar illuminates the target with the radar waves; see Figures 2(c) and 2(d). This type of missiles has a radar receiver that can detect the radar echo returned by the target. It then moves toward the radar return signal via conical sweep for detection. A hybrid homing missile has an infrared seeker head and a microwave radar at the same time. When this missile becomes close enough to the target it turns to perform heat seeking via the head infrared detector [8].

The present work introduces a novel method for the identification of attacking jet fighter targets by the onboard radar of defending homing missiles. The proposed signal processing technique is based on comparing the target feature function that is extracted by processing the received echo to the target signature function that is stored in the radar memory. The radar signature has already been formed by the internal resonances of the cavity-backed aperture raised by the open-ended air-inlet cylindrical pipe of the jet engine. The effect of the additive white Gaussian noise (AWGN) on the performance of the proposed target identification scheme is investigated.

The remaining sections of the present paper can be organized as follows. Section 2 explains the electromagnetic simulation for evaluating the target RCS that is required for simulating the proposed signal processing scheme. This section includes a description of the geometric model of the air-inlet pipe of the jet engine. Section 3 explains the mathematical formulation of the radar signature that is based on the results of electromagnetic simulation concerning the dependence of the RCS on the frequency. Section 4 describes the construction of the radar pulse that is required to distinguish between the various targets. Section 5 provides mathematical formulations to describe the detailed steps of the proposed signal processing chain. In this section a block diagram is presented to illustrate the overall process of target identification. Section 6 provides some numerical examples of the application and examination of the proposed target identification scheme under noisy environment. Finally, Section 7 provides the most important conclusions.

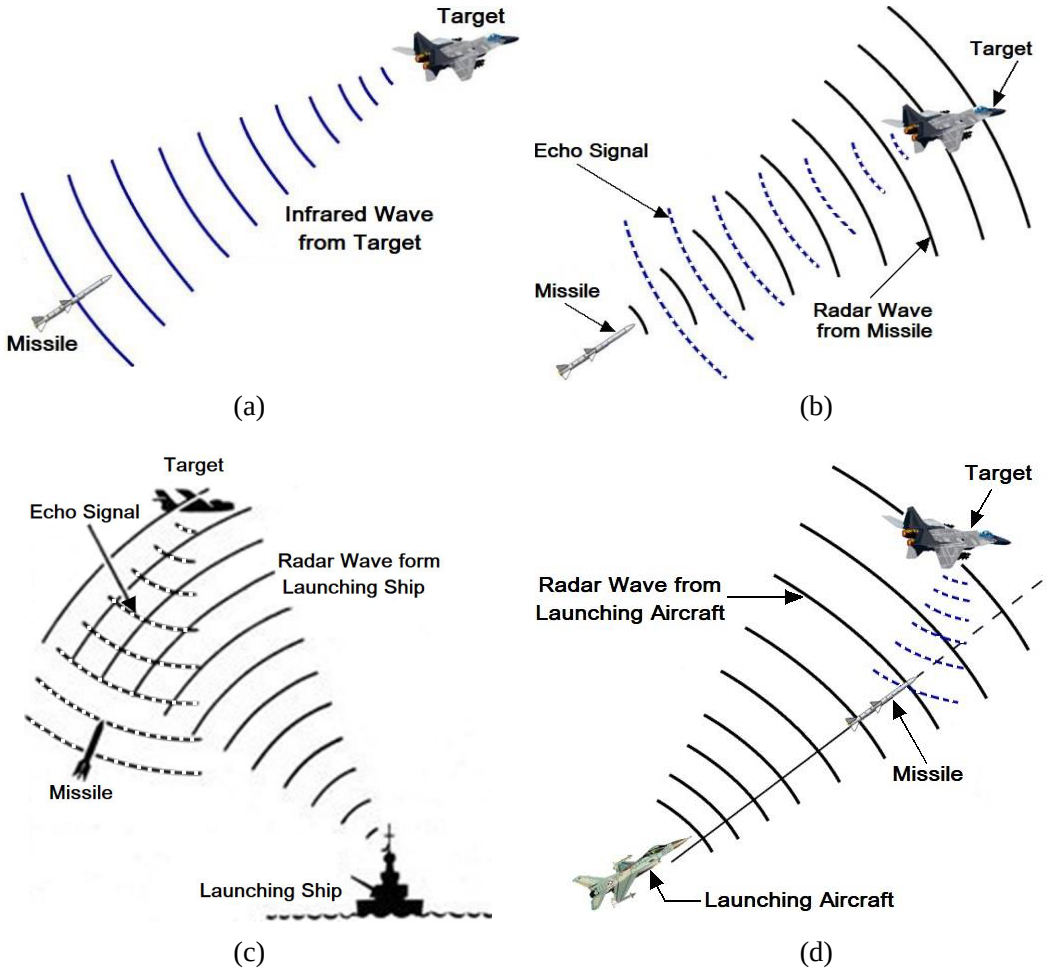

Figure 2. Different types of homing missiles. (a) Passive homing missiles detect the infrared waves emitted from the target. (b) Active homing missiles transmit electromagnetic radar waves and receive the echoes returned from the target. (c) Semi active homing missiles receive the echoes returned from the target illuminated by the ship launching the missile. (d) Semi active homing missiles launched by an aircraft that transmits the radar waves.

2. ELECTROMAGNETIC MODELING AND SIMULATION

This section is concerned with the description of the geometric model used to represent the cylindrical pipe of the jet engine and the electromagnetic simulation for evaluating the RCS due to an incident pulsed plane wave.

2.1. Geometric Model of the Jet Engine Tube of the Fighter Aircraft

The cylindrical pipe existing as terminal parts of jet engines used in the fighter aircrafts for either air inlet or exhaust outlet, see Figure 3, can be modeled as a conducting cylindrical tube that is open-ended at one side [2]. Both the air-inlet and exhaust-outlet pipes can be modeled as backed by a conducting plate [2] at the other end. This is accomplished, in the present work, by closing the other end of the cylindrical tube as shown in Figure 4(a). For exhaust outlet, the pipe aperture may be left blank as shown in Figure 4(b), or a number of radial blades may be used to support the pipe walls as shown in Figure 4(c). For air inlet a number of dynamic radial blades are used to help the air entrance to the jet engine as shown in Figure 4(c). For electromagnetic simulation, a pulsed plane wave with the

Figure 3. Two types of the fighter aircrafts with jet engines. (a) F-15 jet fighter with two jet engine pipes. (b) F-35 jet fighter with one jet engine pipe.

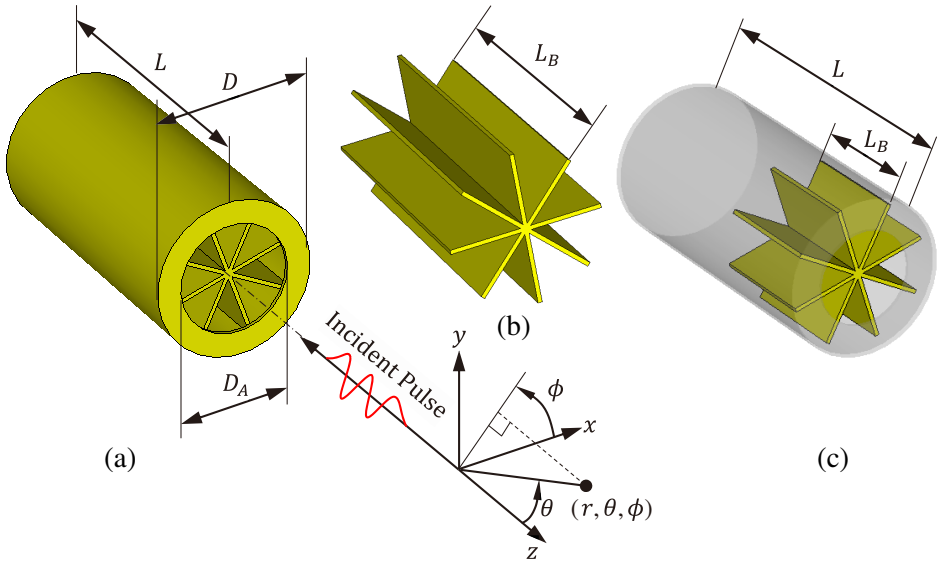

Figure 4. Model of the air inlet pipe of the jet engine in the CST® simulator with the coordinate system and the direction of the incident radar pulse. (a) 3D view showing the pipe at its open end enclosing the radial blades for air inlet. (b) 3D view the eight blades for air inlet. (c) 3D view with a transparent pipe to show the internal blades.

appropriate frequency band is incident on the cavity-backed aperture as shown in Figure 4. The CST® simulator is used to evaluate the RCS and the far field scattering patterns over the frequency band of interest.

The geometric model of the jet engine pipe has the dimensional parameters shown in Figure 4. The conducting cylindrical tube has length L, external diameter D, and internal diameter $(D-2T)$, where T is the metallic wall thickness. Also, the eight radial blades are placed inside the cylindrical cavity near the partially open end and have the same thickness T. The cylindrical tube is closed at one end

and has an aperture of diameter D_A at the other (inlet/outlet) end near which the radial blades are mounted. The number of the blades is N_B, and their length is L_B. Thus, the length of the empty part of the cylinder is $L - L_B$.

2.2. Dependence of the RCS on the Dimensions of the Jet Engine Inlet Pipe

The RCS is obtained using a pulsed plane wave that has been formed as described in Section 3.2. The geometric model of inlet pipe of the jet engine has the shape of a cylindrical tube with eight internal blades as shown in Figure 4. The CST® simulator is used for evaluating the RCS over the frequency band 1.0–2.0 GHz, where the pulsed plane wave is incident on the open-ended side of the pipe model as shown in Figure 4.

The frequency dependence of the RCS of the air inlet pipe model over the frequency band 1.0–2.0 GHz is presented in Figure 5 for different values of the pipe length, L. It is noticed that the RCS as a function of the frequency has multiple sharp minima at the frequencies corresponding to the internal resonance of the cylindrical cavity with the eight conducting blades. Also, it is noticed that the locations of these minima (the resonant frequencies) are considerably affected by the cavity length. It is clear that the number and locations (frequencies) of these minima can be used to uniquely identify the pipe length.

The frequency dependence of the RCS of the inlet pipe over the same frequency band is presented in Figure 6 for different values of the pipe diameter, D. It is noticed that the minima of the RCS as a

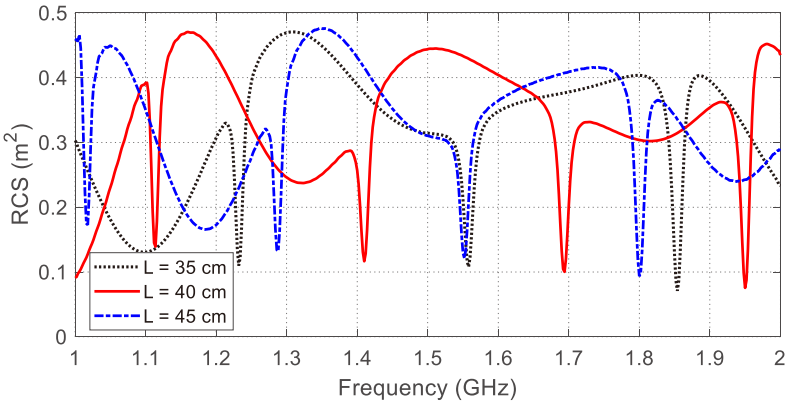

Figure 5. Frequency dependence of the RCS of the air inlet pipe model over the frequency band 1.0–2.0 GHz for different values of the pipe length, L.

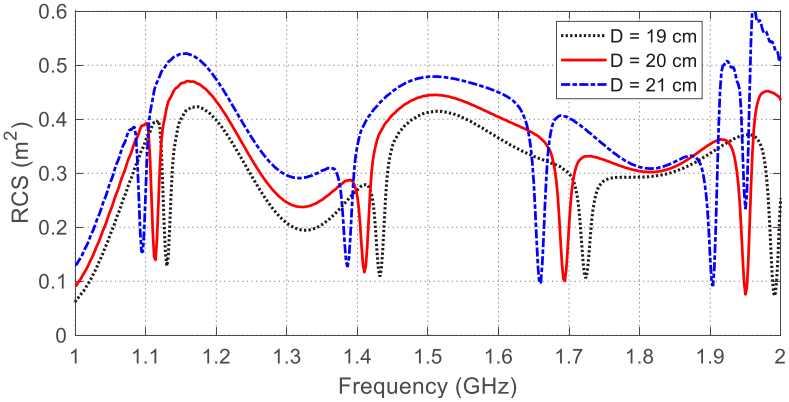

Figure 6. Frequency dependence of the RCS of the air inlet pipe model over the frequency band 1.0–2.0 GHz for different values of the pipe diameter, D.

function of the frequency are shifted towards the left-hand side (i.e., the corresponding frequencies are decreased) with increasing the diameter of the cylindrical cavity. Also, it is obvious that the number of these minima and their corresponding frequencies within the band 1.0–2.0 GHz can be used to uniquely identify the pipe diameter, D.

The aperture diameter, D_A, affects the frequency dependence of the RCS of the inlet pipe as shown in Figure 7. It is noticed that the minima of the RCS as a function of the frequency are shifted towards the right-hand side (i.e., the corresponding frequencies are increased) with increasing the aperture diameter. It may be clear that the number of these minima and their corresponding frequencies within the band 1.0–2.0 GHz can be used to uniquely identify the diameter D_A of the circular aperture at the open end of the inlet pipe.

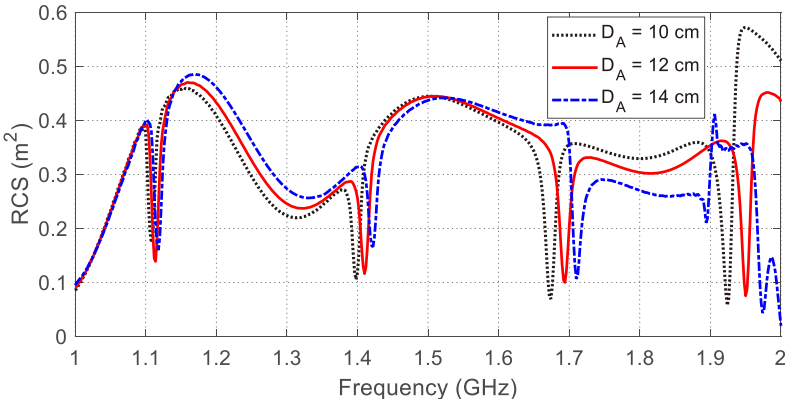

Figure 7. Frequency dependence of the RCS of the air inlet pipe model over the frequency band 1.0–2.0 GHz for different values of the aperture diameter, D_A.

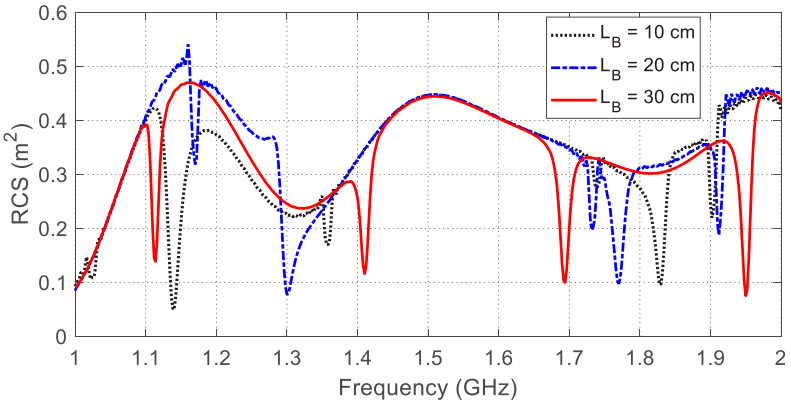

Figure 8. Frequency dependence of the RCS of the air inlet pipe model over the frequency band 1.0–2.0 GHz for different values of the blade length, L_B.

The frequency dependence of the RCS of the inlet pipe is affected by the length L_B along which the blades extend inside the cylindrical cavity shown in Figure 8. It is noticed that the frequencies of the RCS minima (i.e., the internal resonance frequencies) are strongly affected by the length of blades. It may be clear that the number of these minima and their corresponding frequencies within the band 1.0–2.0 GHz can be used to uniquely identify the length L_B of the radial blades placed near the aperture of the air inlet/exhaust outlet of the jet engine pipe.

The above results obtained by the CST® simulator are examples to show how the resonant frequencies of the jet engine pipe interior can be accurately determined through electromagnetic simulation. It should be noted that the air inlet pipe of the various types of the jet fighters have

the common construction described in Section 2.1. However, the dimensions of the geometric model of the different types are not the same. The dimensions of the model described in Section 2.1 for a specific jet fighter type can be used to distinguish this type from the others. Based on the knowledge of the detailed dimensions of the jet engine pipe of a specific jet fighter, the complete parametric studies like those presented above are required to formulate the interior signature function of this target. The method proposed to construct the target signature using the above simulation results is explained in Section 3.

2.3. Far Field Scattering Patterns

It may be useful to study the shape of the scattered field patterns in the far zone upon the incidence of a pulsed plan wave as described above. Figure 9 presents the scattered field patterns for an air inlet pipe that has the dimensions $L = 40\,\text{cm}$, $D = 20\,\text{cm}$, and $D_A = 12\,\text{cm}$ at the four frequencies corresponding to the internal resonances encountered within the frequency band 1.0–2.0 GHz. It should be noted that the plane wave propagation direction is parallel to the cylinder axis and is incident directly on the circular aperture. It is clear that the scattering patterns at the four frequencies have their maxima in the forward and backward directions and their minima on the side directions. Also, it is noticed that the scattering beam becomes narrower with increasing the frequency.

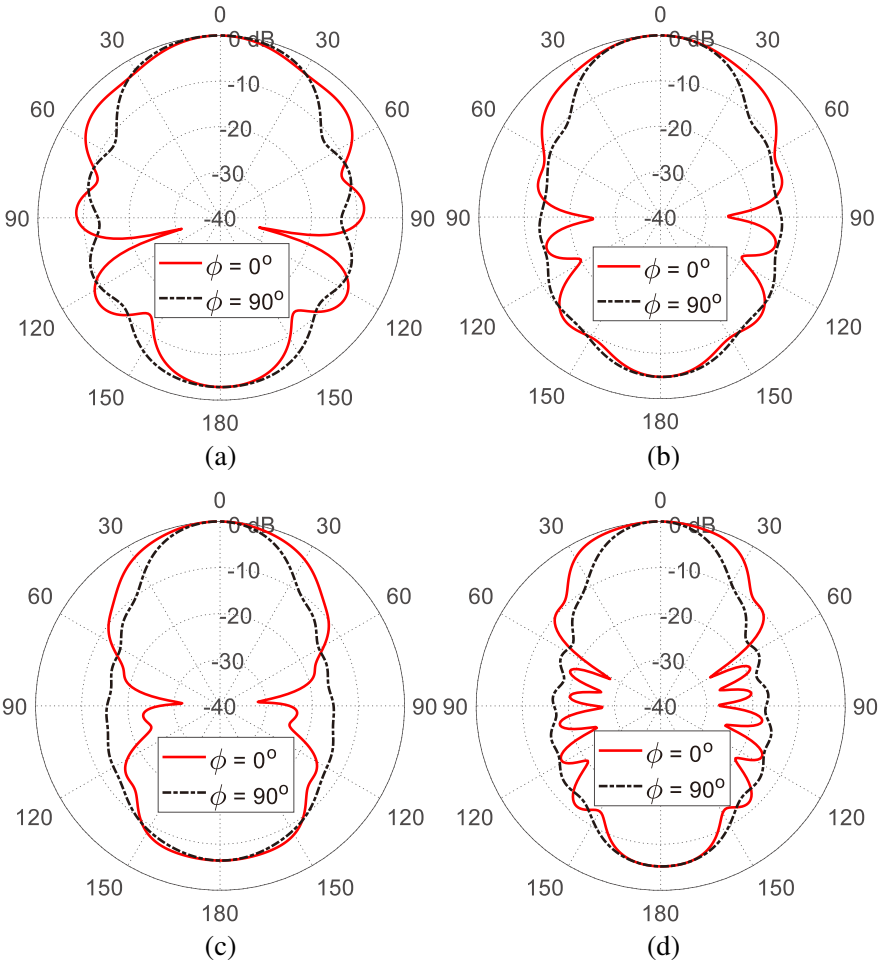

Figure 9. Far field scattering patterns due to a pulsed plane wave incident on a cylindrical model of jet engine pipe with circular aperture and eight blades as that shown in Figure 4. The air inlet pipe has the dimensions $L = 40\,\text{cm}$, $D = 20\,\text{cm}$, and $D_A = 12\,\text{cm}$. (a) $f = 1200\,\text{MHz}$, (b) $f = 1418\,\text{MHz}$, (c) $f = 1912\,\text{MHz}$, (d) $f = 1958\,\text{MHz}$.

3. FORMULATION OF INTERIOR SIGNATURE FUNCTION

Let the resonant frequency of the interior (cavity) of the air inlet pipe corresponding to the n^{th}-order mode of the internal cavity of the engine pipe with the eight blades be designated as f_{C_n}. The resonant frequencies of the pipe interior are expected to be close to the resonant frequencies of the closed cylindrical cavity of the same dimension, $\hat{f}_{C_n}$, $n = 1, 2, ...$ which can be calculated using the following expression [M01, M02].

$$f_{C_n} \cong \hat{f}_{C_n} = \frac{c}{2\pi\sqrt{\mu_r \epsilon_r}} \sqrt{\left(\frac{2k_{mq}}{D}\right) + \left(\frac{p\pi}{L}\right)} \tag{1}$$

where c is the speed of light; q, m, and p are the mode integers; k_{mq} is the q^{th} root of the m^{th}-order Bessel function of the first kind; D and L are the diameter and length of the cylindrical cavity, respectively; and μ_r and ϵ_r are the relative permeability and permittivity of the material filling the cylindrical cavity, respectively.

The exact cavity resonant frequencies f_{C_n}, $n = 1, 2, ...$ of the pipe interior can be evaluated through electromagnetic simulation or experimental work. The knowledge of the internal resonant frequencies, f_{C_n}, $n = 1, 2, ...$, for a specific air inlet pipe, is enough to formulate the signature function $S(f)$ of this target as follows.

$$S(f) = \sum\nolimits_n \delta(f - f_{C_n}) \tag{2}$$

Note that the resonant frequencies f_{C_n}, $n = 1, 2, ...$, can be obtained as the locations (frequencies) of the peaks of the function $G(f)$.

4. CONSTRUCTION OF THE DISTINGUISHING RADAR PULSE

The radar pulse should cover the frequency band within which the distinguishing internal resonances of the air inlet pipe cavity of the jet engine exist so that the effect of these resonances might appear in the echo signal. In other words, a compressed radar pulse that includes the required frequency content can be used for efficient detection, classification, and identification of the detected flying fighter jet or the target that the missile is looking for. A frequency-chirped rectangular pulse can be used as the radar pulse for this purpose [9]. Such a pulse can have the following general expression.

$$p(t) = \text{rect}\left(\frac{t - t_0 - T/2}{T}\right) \sin\theta(t) \tag{3}$$

where t_0 and T are the start time and duration of the radar pulse, respectively, and $\theta(t)$ is the instantaneous value of the angle of the sinusoidal function.

The linear frequency modulation (LFM) can be used for chirping the radar square pulse by expressing the angle $\theta(t)$ as follows.

$$\theta(t) = 2\pi\left[\frac{B}{2T}(t - t_0)^2 + \left(f_C - \frac{B}{2}\right)(t - t_0)\right] \tag{4}$$

where f_C is the center frequency of the operational frequency band of the radar pulse.

The instantaneous frequency (as a function of time) of the chirped pulse using LFM can be expressed by differentiating the angle $\theta(t)$ with respect to time as follows.

$$f_i(t) = \frac{\partial\theta(t)}{\partial t} = \frac{B}{T}(t - t_0) + f_C - \frac{B}{2} \tag{5}$$

The minimum frequency component of the transmitted pulse, f_S, can be obtained by setting $t = t_0$ in (3), which gives the following expression.

$$f_S = f_C - \frac{B}{2} \tag{6}$$

The maximum frequency component of the transmitted pulse, f_E, can be obtained by setting $t = T + t_0$ in (3), which gives the following expression.

$$f_E = f_C + \frac{B}{2} \tag{7}$$

For example, to get the bandwidth of the radar pulse equal to 1 GHz and to include the frequencies from $f_S = 1\,\text{GHz}$ to $f_E = 2\,\text{GHz}$, one sets $B = 1\,\text{GHz}$ and $f_C = 1.5\,\text{GHz}$. Using these values, the chirped radar pulse can be formed using expression (1). For such radar pulse of duration $T = 50\,\text{ns}$ and starting at $t = t_0 = 25\,\text{ns}$, the envelop of the pulse is shown in Figure 10(a); the instantaneous frequency is linearly increasing with time as shown in Figure 10(b); the radar chirped pulse is presented in Figure 10(c); the spectrum of the radar pulse is presented in Figure 10(d) showing a magnitude of flat response over the frequency band 1.0–2.0 GHz. For simulation of the radar signal preprocessing, the time is sampled with sampling frequency $100 f_C$ which corresponds to a sampling period $\Delta t = 6.67\,\text{ps}$ and frequency sweep resolution $\Delta f = 10\,\text{MHz}$.

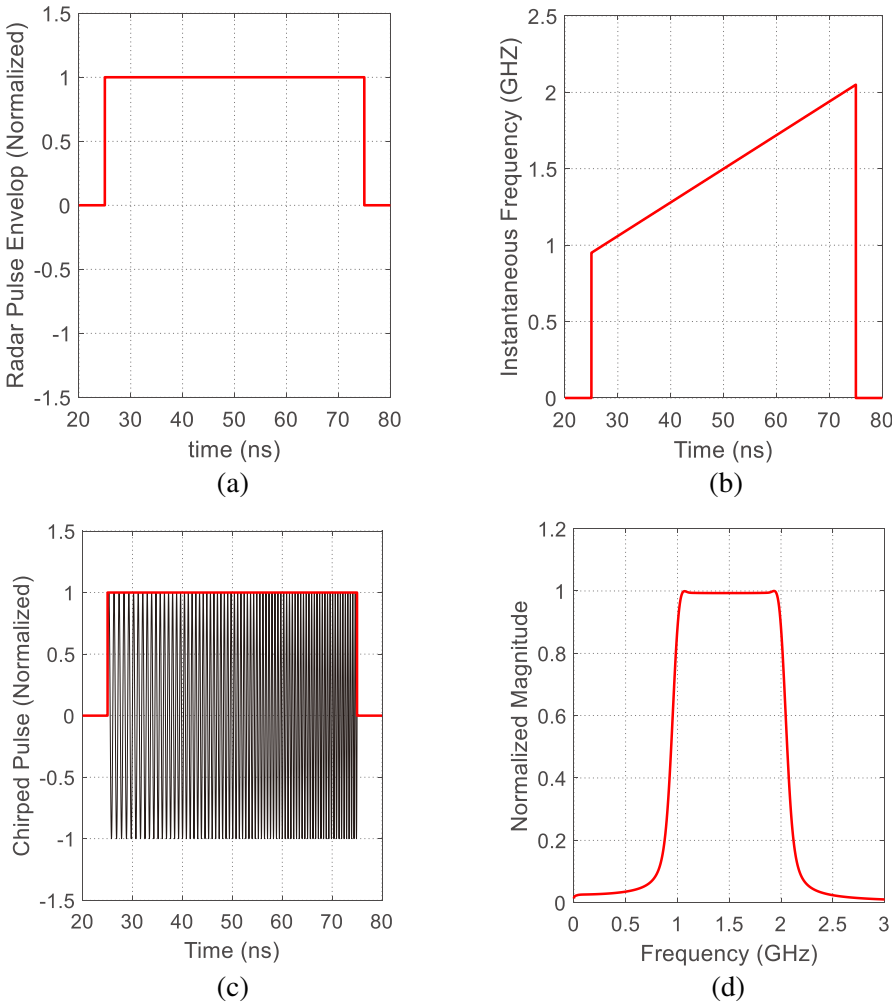

Figure 10. Formation of the radar pulse to include the frequency band (1.0–2.0 GHz). (a) Rectangular envelop of the radar pulse showing pulse width of 50 ns. (b) The instantaneous frequency as a function of time over the duration of the radar pulse. (c) The final time waveform of the chirped radar pulse. (d) The spectrum of the radar pulse showing a flat response over the desired frequency band (1.0–2.0 GHz).

5. PROPOSED SIGNAL PROCESSING CHAIN FOR MAKING USE OF INTERIOR RESONANCE CONTRIBUTION TO THE RCS FOR TARGET IDENTIFICATION

This section is concerned with describing the radar signal processing required for classification and identification of the homing missile (fighter jet) targets comprising cylindrical cavity-backed apertures of the jet engine pipe for air inlet or exhaust outlet.

5.1. Matched Filter Processing of the Received Signal

Let $\sigma(t)$ be the echo signal arriving at the receiver input, i.e., after being amplified by the low noise amplifier (LNA). For maximum signal-to-noise ratio (SNR), a matched filter is placed in the receiver just after the LNA. The impulse response of the matched filter, $h(t)$, has the same time waveform as that of the transmitted pulse, $p(t)$, which is given by (1). Thus, the impulse response of the receiver matched filter has the following expression.

$$h\left(t\right) = \text{rect}\left(\frac{t - t_0 - T/2}{T}\right) \sin\theta(t) \tag{8}$$

The transfer function of the matched filter, $H(f)$, is the Fourier transform of $h(t)$ and can be obtained in a digital processing unit by applying the fast Fourier transform to the (discrete) time samples of $h(t)$.

$$H\left(f\right) = \text{FFT}(h) \tag{9}$$

In the time domain, the received signal, $r_i(t)$, at the input of the matched filter can be expressed as follows.

$$r_i\left(t\right) = \sigma_i\left(t\right) + \nu_i\left(t\right) = G_{\text{LNA}}\left[\sigma\left(t\right) + \nu(t)\right] \tag{10}$$

where $\sigma(t)$ is the received echo signal, $\nu(t)$ the instantaneous value of the AWGN at the input of the LNA, and G_{LNA} the gain of the LNA. Thus, $\sigma_i(t) + \nu_i(t)$ is the echo signal associated with AWGN at the input of the LNA the matched filter.

In the time domain, the signal at the output of the matched filter can be obtained by performing the convolution between the impulse response of the matched filter, $h(t)$, and the echo signal associated with the noise, $[\sigma_i(t) + \nu_i(t)]$, as follows.

$$r\left(t\right) = G_{\text{LNA}} h(t) * \left[\sigma\left(t\right) + \nu(t)\right] \tag{11}$$

The spectrum of the received echo, $\Sigma_i(f)$, at the matched filter input can be obtained by applying the FFT to the time discretized (sampled) version of $\sigma_i(t)$ as follows.

$$\Sigma_i\left(f\right) = G_{\text{LNA}}\,\text{FFT}\left[\sigma\left(t\right)\right] \tag{12}$$

For simulation, Gaussian random sequences can be generated to represent the discrete-time values (samples) of the noise, $\nu(t)$. To get a frequency-domain expression for the received signal associated with the AWGN, the discrete-time sequences of $\nu(t)$ can be transformed to the frequency domain as follows.

$$\mathcal{N}_i\left(f\right) = G_{\text{LNA}}\,\text{FFT}\left[\nu\left(t\right)\right] \tag{13}$$

It is assumed that the AWGN has uniform power spectral density, N_0, over the frequency band of the received signal and, hence, it can be considered that the following condition should be satisfied when generating the Gaussian random sequence of noise samples.

$$\left|\mathcal{N}_i(f)\right|^2 = G_{\text{LNA}}^2 N_0 \tag{14}$$

In the frequency domain, expression (10) can be formulated as follows.

$$R\left(f\right) = H\left(f\right)\left[\Sigma_i\left(f\right) + \mathcal{N}_i(f)\right] \tag{15}$$

The frequency-domain evaluation of the matched-filter processed version of the received echo signal (associated with AWGN) through expression (14) can be used instead of time-domain evaluation through expression (10) to obtain the signal $R(f)$ at the matched filter output in a much simpler and more computationally efficient way.

5.2. Evaluation of the Normalized Strength Function

Once the matched-filter processed version of the received echo signal, $R(f)$, the feature extraction can be achieved by generating the feature function. For this purpose, let us define the strength function $g(f)$ as follows.

$$g\left(f\right) = \left|\frac{\partial R\left(f\right)}{\partial f}\right| \tag{16}$$

As the signal $R(f)$ is the spectrum of the echo signal that is backscattered by the target it has the same frequency dependence as the RCS of this target. It is well known that the RCS, as a function of the frequency, has very sharp minima at the frequencies corresponding to the internal resonances of the air inlet pipe interior. At the resonant frequencies the internal modes are excited inside the pipe cavity leading to considerable absorption (storage) of the incident power into the cavity, which causes dramatic reduction of the backscattered power at these frequencies. Thus, the RCS, as a function of the frequency, has sharp minima, i.e., considerable reduction over very narrow bands, around the internal resonant frequencies. Accordingly, the differentiation in (15) has sharp peaks at these frequencies, and hence, the function $g(f)$ expresses the strength (sharpness) of the RCS-frequency curve at each resonance. The normalized strength function can be expressed as the normalized version of $g(f)$ as follows.

$$G\left(f\right) = \frac{g\left(f\right)}{\max\left[g\left(f\right)\right]} \tag{17}$$

5.3. Formulation of the Interior Feature Function

The target feature can be extracted by processing the echo signal at the radar receiver. The process of feature extraction can be achieved by construction of the interior feature function. This can be performed by getting the locations (frequencies) of the peaks, f_{P_n}, $n = 1, 2, 3, ...$ of the normalized strength function $G(f)$. Thus, the feature function, $\mathcal{F}(f)$, of the air inlet pipe interior can be formulated as follows.

$$\mathcal{F}\left(f\right) = \sum\nolimits_n \text{rect}\left(\frac{f - f_{P_n}}{\Delta f}\right) \tag{18}$$

where Δf is the sweep frequency resolution used in the formation of the radar pulse as described in Section 4.

5.4. Target Classification and Identification

The detected target can be recognized or denied upon the calculation of two important quantities $\mathcal{J}$ and $\mathcal{D}$. The quantity $\mathcal{J}$ is defined as follows.

$$\mathcal{J} = \prod\nolimits_n \int_{f_S}^{f_E} \mathcal{F}\left(f\right) \delta\left(f - f_{C_n}\right) \, df \tag{19}$$

The quantity $\mathcal{D}$ is defined as follows.

$$\mathcal{D} = \int_{f_S}^{f_E} \mathcal{F}\left(f\right) S\left(f\right) df \tag{20}$$

The quantity $\mathcal{J}$ represents the decision whether the target is identified or unidentified. In other words, if $\mathcal{J} = 1$, then the target is identified, i.e., the detected object is the target that the missile is looking for, whereas, if $\mathcal{J} = 0$, then the target is unidentified, i.e., the detected object is not the target that the missile is looking for.

The quantity $\mathcal{D}$ represents the distance between the feature of the detected object and the signature of the target that the missile is looking for. This quantity is more useful for target classification rather than target identification.

5.5. Block Diagram of the Proposed Signal Processing Chain

The signal processing chain of the received signal that is backscattered to the monostatic radar antenna has been described in the Sections 5.1 through 5.4. This processing chain can be illustrated using the block diagram presented in Figure 11 for the radar receiver. This scheme can be used by homing missiles for recognizing and tracking the jet fighter targets.

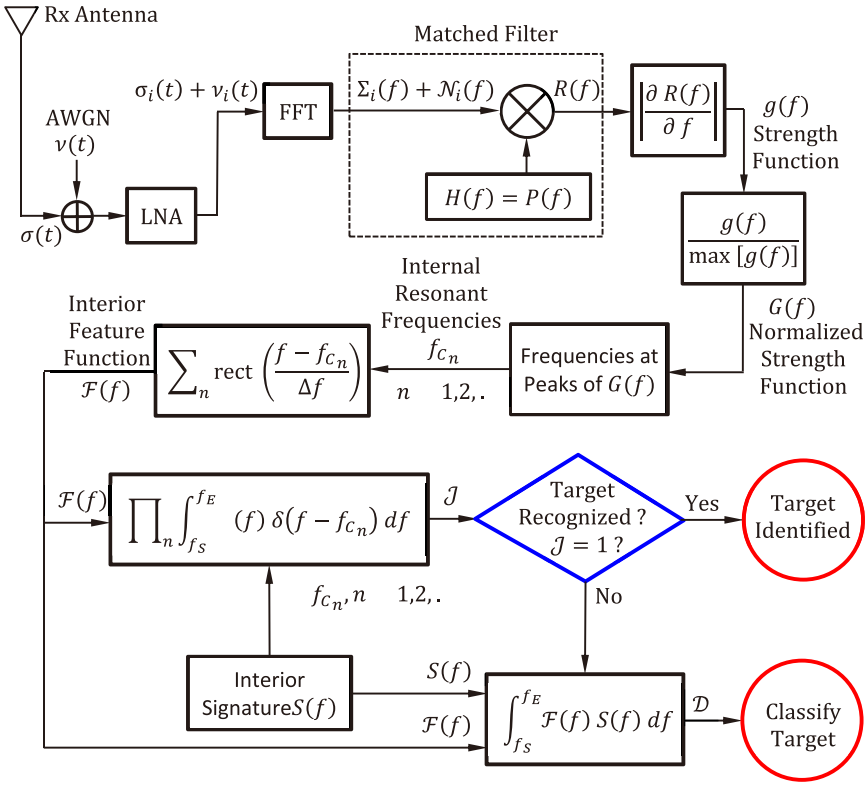

Figure 11. The signal processing chain in the homing missiles radar receiver for the proposed target identification and classification scheme of jet fighters based on the signature of the air inlet pipes of the jet engine.

6. NUMERICAL EXAMPLES FOR APPLICATION OF THE PROPOSED SIGNAL PROCESSING CHAIN FOR FEATURE EXTRACTION AND TARGET IDENTIFICATION

The numerical results presented in this section is concerned with examining the procedure of signal processing proposed in Section 2 when being applied to identify the target of a missile seeking for a specific jet fighter. Assume that there are two targets (T_1 and T_2) with their inlet pipes that can be modeled as described in Section 3.1. Both the targets have pipes of diameter $D = 20\,\text{cm}$, and aperture diameter $D_A = 12\,\text{cm}$. The difference between them is that target T_1 has a pipe length $L_1 = 40\,\text{cm}$ and blades length $L_B = 30\,\text{cm}$, whereas target T_2 has a pipe length $L_2 = 35\,\text{cm}$ and blades length $L_B = 25\,\text{cm}$.

6.1. Simulation Results for RCS-Frequency Dependence and Construction of the Interior Signature Functions

The simulation results for the variation of the RCS of the targets T_1 and T_2 with the frequency over the band 1.0–2.0 GHz are presented in Figures 12(a) and 12(b), respectively, in comparison to the RCS

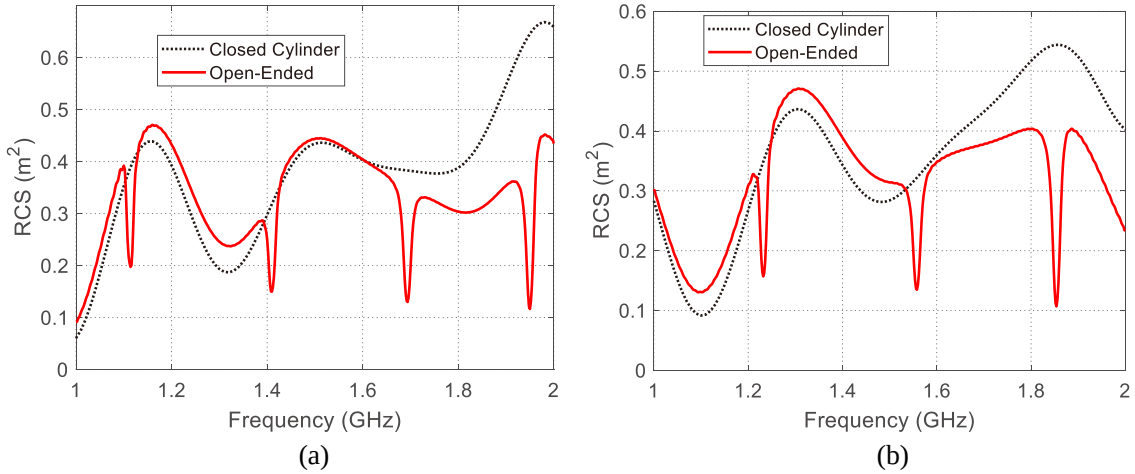

Figure 12. Frequency dependence of the RCS of two air inlet pipes of the model (shown in Figure 4) over the frequency band 1.0–2.0 GHz compared with RCS of a solid conducting cylinder of the same external dimensions. The inlet pipes ha internal diameter $D = 20\,\text{cm}$, aperture diameter $D_A = 12\,\text{cm}$, (a) pipe length $L = 40\,\text{cm}$, and blades length $L_B = 30\,\text{cm}$ for target T_1, (b) pipe length $L = 35\,\text{cm}$, and blades length $L_B = 25\,\text{cm}$ for the target T_2.

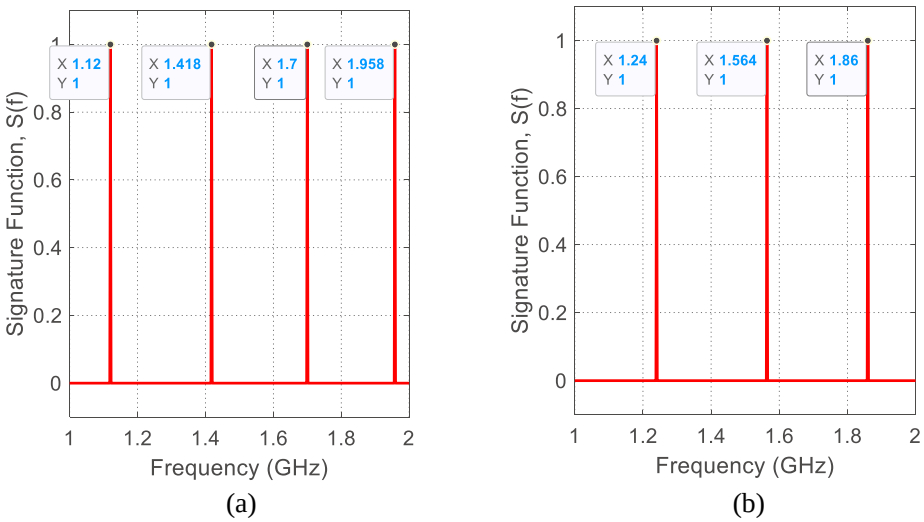

Figure 13. Interior signature functions of the air inlet pipe model (shown in Figure 4) over the frequency band 1.0–2.0 GHz constructed from RCS-frequency curve obtained by simulation (presented in Figure 12) for the targets T_1 and T_2. (a) Signature $S_1(f)$ for T_1 that has a pipe of length $L = 40\,\text{cm}$ and blades of length $L_B = 30\,\text{cm}$. (b) Signature $S_2(f)$ for T_2 that has a pipe of length $L = 35\,\text{cm}$ and blades of length $L_B = 25\,\text{cm}$.

of a solid cylinder of the same external dimensions (length and diameter). It is shown that, for the target T_1, the RCS of the open-ended cylinder representing the jet inlet pipe with their internal eight blades has four sharp minima corresponding to the resonances of the internal cavity existing within the frequency band 1.0–2.0 GHz. For the second target, T_2, the RCS has three sharp minima corresponding to the internal resonances within the same frequency band.

From the simulation results presented in Figure 12, the interior signature functions, $S_1(f)$ and $S_2(f)$, for the targets T_1 and T_2, respectively, are presented in Figures 13(a) and 13(b). It should be noted that these signature functions have been obtained by applying the method described in Section 3.

6.2. Application of the proposed Processing Chain to the Received Echo Signal

This section is concerned with the presentation and discussion of the results of applying the signal processing chain (detailed in Section 5 and illustrated by the block diagram presented in Figure 11) to the radar echo scattered from the target jet fighter and returned back to the receiver antenna. The results are concerned with targets T_1 and T_2 as mentioned in the introductory paragraph of Section 6. It should be noted that the echo signal has been obtained by electromagnetic simulation due to the incidence of a radar pulse, $p(t)$, (constructed as described in Section 4) on the air inlet pipe model (presented in Figure 4) over the frequency band 1.0–2.0 GHz.

For target T_1, Figure 14(a) presents the normalized magnitude of the received echo signal spectrum, $|R_1(f)|$, after being processed by the matched filter of the receiver. The normalized strength function, $G_1(f)$, is obtained as described in Section 5.2 and presented in Figure 14(b). The interior feature function, $\mathcal{F}_1(f)$, is extracted as described in Section 5.3 and is presented in Figure 14(c). Note that the interior signature function, $S_1(f)$, of the target T_1 is presented in Figure 13(a) and constructed as explained in Section 3. In this case, it is assumed that SNR = 30 dB, which is large enough to get correct target identification decision after processing the received echo. It is clear that the locations (frequencies) of the Dirac-delta functions constructing $G_1(f)$ are the same as the locations of the sharp minima of the frequency-RCS curve presented in Figure 12(a). Hence, the extracted interior function feature, $\mathcal{F}_1(f)$, presented in Figure 14(c) matches the interior signature function, $S_1(f)$, plotted in Figure 13(a). This means that the proposed signal processing scheme for target identification results in "hit" decision since the application of (18), in this case, results in $\mathcal{J} = 1$, which is the correct decision.

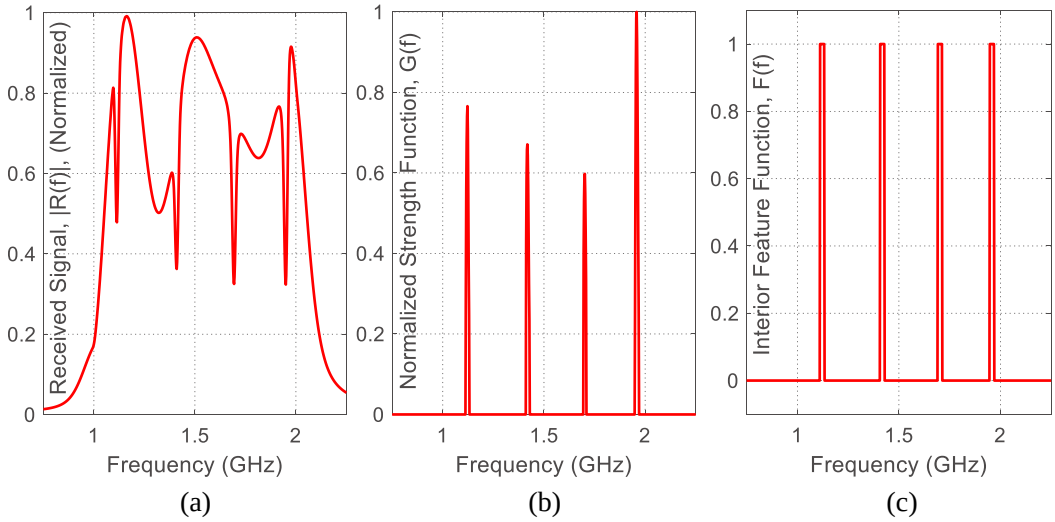

Figure 14. Stages of the received echo signal processing in the radar receiver for SNR = 30 dB due to the incidence of the radar pulse, $p(t)$ described in Section 4, over the frequency band 1.0–2.0 GHz on the target T_1. (a) Normalized magnitude of the signal spectrum, $|R_1(f)|$, at the matched filter output. (b) The extracted normalized strength function, $G_1(f)$. (c) The extracted interior feature function, $\mathcal{F}_1(f)$.

The same procedure is repeated for testing the process of identifying the target T_2. Figure 15(a) presents the normalized magnitude of the received echo signal spectrum, $|R_2(f)|$, after being processed by the matched filter of the receiver. The normalized strength function, $G_2(f)$, is presented in Figure 15(b), and the interior feature function, $\mathcal{F}_2(f)$, is presented in Figure 15(c). It is considered that the SNR = 30 dB, which is large enough to get the locations (frequencies) of the Dirac-delta functions constructing $G_2(f)$ identical to the locations of the sharp minima of the frequency-RCS curve presented in Figure 12(b). Hence, the extracted interior function feature, $\mathcal{F}_2(f)$, presented in Figure 15(c) matches the interior signature function, $S_2(f)$, plotted in Figure 13(b). This means that the proposed signal processing for target identification results in "hit" decision since the application of (18), in this case, results in $\mathcal{J} = 1$, which is the correct decision.

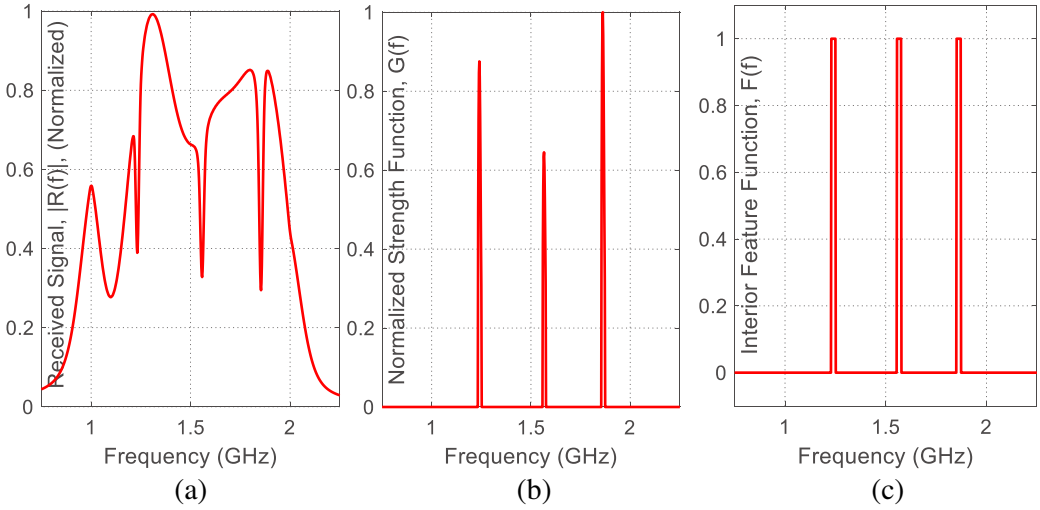

Figure 15. Stages of the received echo signal processing in the radar receiver for SNR = 30 dB due to the incidence of the radar pulse, $p(t)$ described in Section 4, over the frequency band 1.0–2.0 GHz on the target T_2. (a) Normalized magnitude of the signal spectrum, $|R(f)|$, at the matched filter output. (b) The extracted normalized strength function, $G_2(f)$. (c) The extracted interior feature function, $\mathcal{F}_2(f)$.

6.3. Effect of the Noise on the Proposed System Performance

The application of the signal processing technique for jet fighter target identification by homing missiles has been described in detail in Section 5, and two numerical examples have been presented and discussed for the application of this technique to identify the jet fighter targets T_1 and T_2 described above. However, the two examples have been presented under the assumption that the SNR = 30 dB, which is large enough to get correct target identification decision. In this section, lower values of the SNR are considered in order to investigate the effect of the AWGN on the performance of the proposed scheme.

Considering that the AWGN encountered at the receiver results in SNR of 15 dB, the normalized magnitude of the processed echo signal spectrum, $|R_1(f)|$, is that presented in Figure 16(a). The

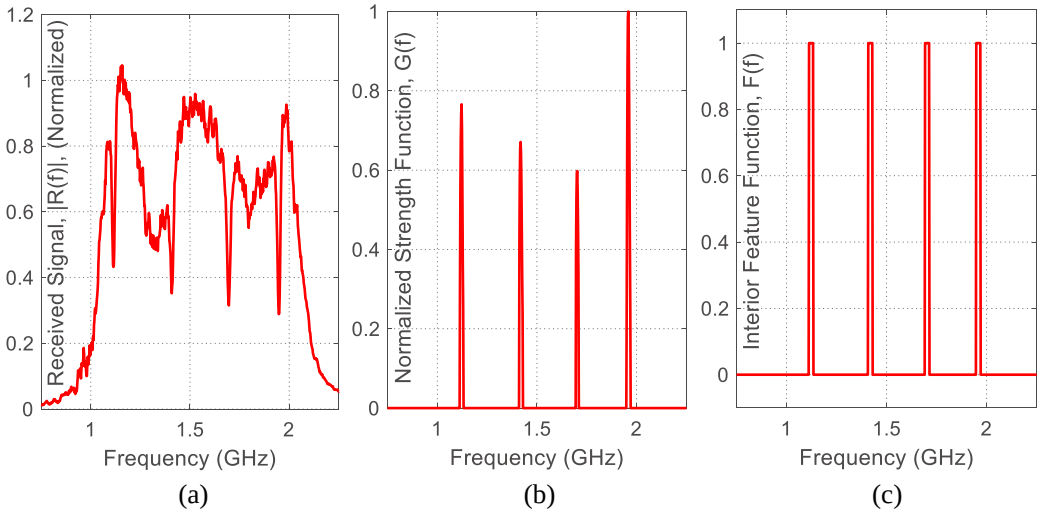

Figure 16. Stages of the received echo signal processing in the radar receiver for SNR = 15 dB due to the incidence of the radar pulse, $p(t)$ described in Section 4, over the frequency band 1.0–2.0 GHz on the target T_1. (a) Normalized magnitude of the signal spectrum, $|R(f)|$, at the matched filter output. (b) The extracted normalized strength function, $G_1(f)$. (c) The extracted interior feature function, $\mathcal{F}_1(f)$.

corresponding normalized strength function, $G_1(f)$, and the interior feature function, $\mathcal{F}_1(f)$, are presented in Figures 16(b) and 16(c), respectively. Despite that the received signal magnitude, $|R_1(f)|$, is clearly affected by the noise, it is found, by comparing Figures 16(b) and 16(c) to Figures 14(b) and 14(c), respectively, that both the normalized strength function, $G_1(f)$, and the interior feature function, $\mathcal{F}_1(f)$, are not affected by the reduction of the SNR from 30 dB to 15 dB. Thus, the proposed signal processing for target identification is still capable to correctly identify the target T_1.

However, when the SNR is further reduced to 5 dB, the received signal spectrum, $|R_1(f)|$, is considerably affected by the noise as shown in Figure 17(b). By comparing Figures 17(b) and 17(c) to Figures 14(b) and 14(c), respectively, it is found that both the normalized strength function, $G_1(f)$,

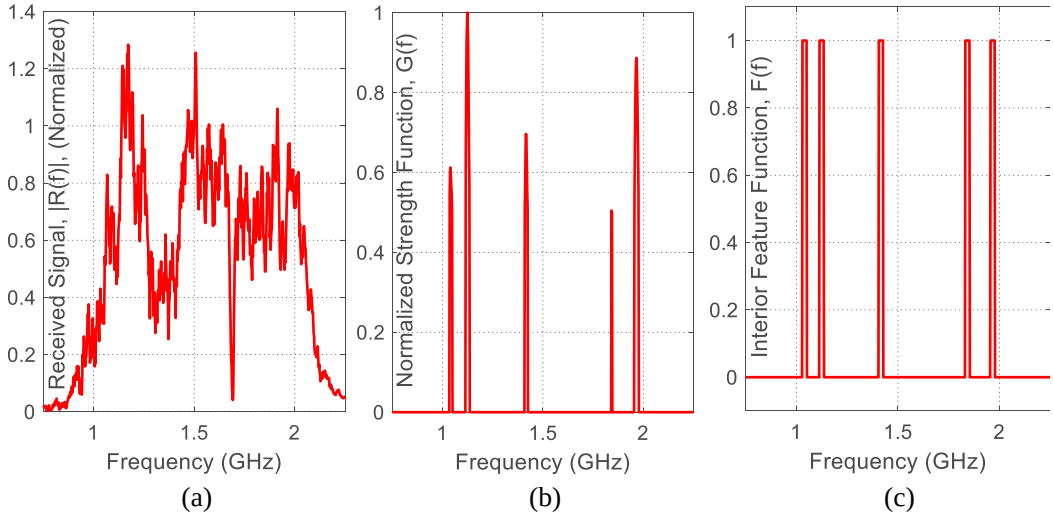

Figure 17. Stages of the received echo signal processing in the radar receiver for SNR = 5 dB due to the incidence of the radar pulse, $p(t)$ described in Section 4, over the frequency band 1.0–2.0 GHz on the target T_1. (a) Normalized magnitude of the signal spectrum, $|R(f)|$, at the matched filter output. (b) The extracted normalized strength function, $G_1(f)$. (c) The extracted interior feature function, $\mathcal{F}_1(f)$.

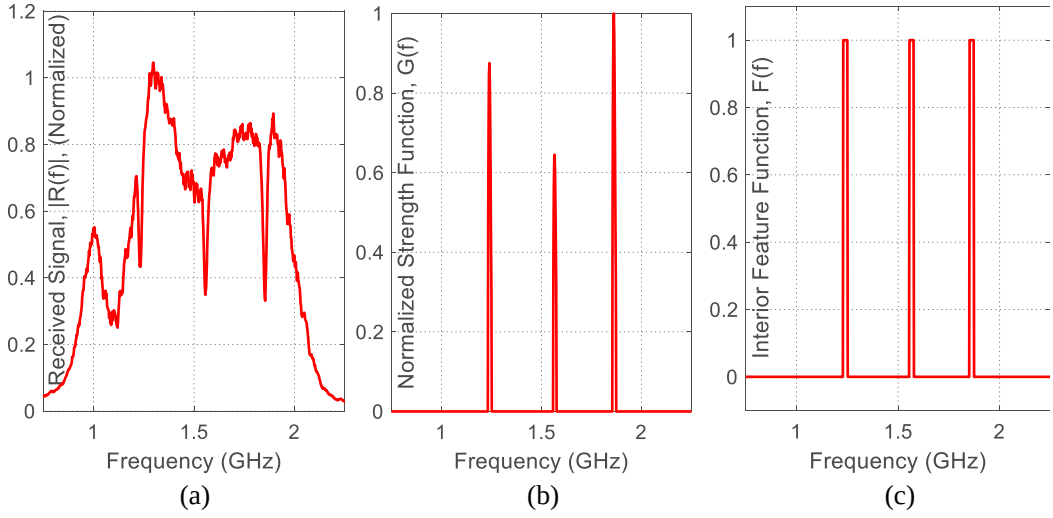

Figure 18. Stages of the received echo signal processing in the radar receiver for SNR = 15 dB due to the incidence of the radar pulse, $p(t)$ described in Section 4, over the frequency band 1.0–2.0 GHz on the target T_2. (a) Normalized magnitude of the signal spectrum, $|R(f)|$, at the matched filter output. (b) The extracted normalized strength function, $G_2(f)$. (c) The extracted interior feature function, $\mathcal{F}_2(f)$.

and the interior feature function, $\mathcal{F}_1(f)$, are negatively affected by reducing the SNR leading to obvious mismatch between the target signature, $S_1(f)$, and the extracted feature, $\mathcal{F}_1(f)$, which in turn results in missing the target due to the excessive noise.

Another example to investigate the effect of increasing the AWGN on the capability of the proposed signal processing technique to correctly identify the jet fighter targets is presented in Figures 18 and 19, where the missile is seeking for target T_2, and the SNR is considered to be 15 dB and 5 dB, respectively. Like the situation with target T_1 investigated in the previous example, the proposed signal processing technique succeeds to identify the target when the SNR is 15 dB and fails when the SNR is 5 dB.

One of the most important measures to evaluate the performance of the proposed signal processing scheme when it is applied to identify the jet fighter targets is the false alarm rate (FAR). Let us define the FAR as the probability of the wrong target identification decisions under noisy conditions. In the present investigation, to evaluate the FAR, for each value of the SNR, the proposed signal processing scheme has been repeated for 100 times. In this experiment, the percent FAR is equal to the number of

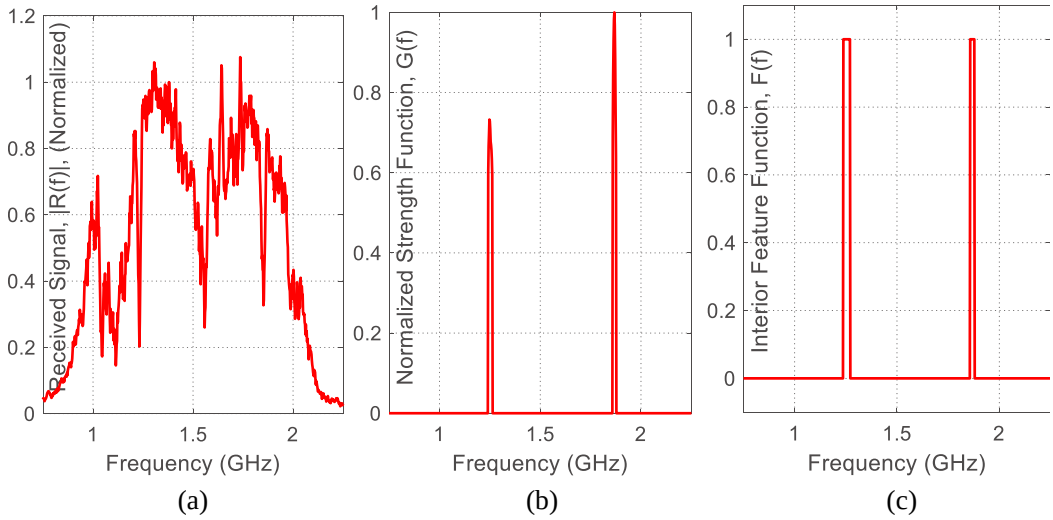

Figure 19. Stages of the received echo signal processing in the radar receiver for SNR = 5 dB due to the incidence of the radar pulse, $p(t)$ described in Section 4, over the frequency band 1.0–2.0 GHz on the target T_2. (a) Normalized magnitude of the signal spectrum, $|R(f)|$, at the matched filter output. (b) The extracted normalized strength function, $G_2(f)$. (c) The extracted interior feature function, $\mathcal{F}_2(f)$.

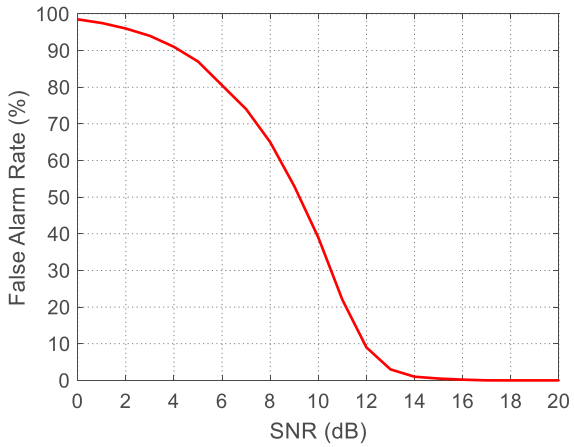

Figure 20. Dependence of the percent FAR of the proposed target identification shceme on the SNR considering the AWGN associating the radar echo signal at the input of the LNA of the radar receiver.

wrong target identification decisions. The dependence of the percent FAR on the SNR at the input of the receiver matched filter is presented in Figure 20. Through these results, it is shown that the target identification algorithm proposed for active homing missiles seeking for jet fighter targets succeeds to take the correct decisions in the majority of the test cases whenever the SNR is greater than 12 dB.

7. CONCLUSION

A novel signal processing scheme has been proposed for the identification of jet fighter targets by the onboard radar of homing missiles. The proposed scheme is based on the interior signature function that is formed by the knowledge of the internal resonant frequencies of the cavity-backed apertures raised by the air-inlet pipes of the jet engine. These pipes have been modeled as open ended conducting cylinders with internal radial conducting blades placed in the cylindrical cavity near the open end of the cavity. A chirped radar pulse has been constructed by applying LFM to include the frequencies within the band 1.0–2.0 GHz with a frequency sweep resolution that is high enough to capture all the internal resonance within this band. The CST® simulator has been employed to get the RCS of the air-inlet pipe model as a function of the frequency where the pulsed plane wave is formulated as mentioned above. The proposed target identification algorithm has been mathematically formulated and computationally applied to identify air-inlet pipe targets with different dimensions. The AWGN has been modeled, and its effect on the performance of the proposed target identification scheme has been numerically investigated. Some numerical examples have been presented for examination of the proposed signal processing scheme. It has been shown that the proposed algorithm succeeds to take the correct target identification decision with FAR lower than 10% for SNR higher than 12 dB.

REFERENCES

1. Hussein, K. F. A., "Effect of internal resonance on the radar cross section and shield effectiveness of open spherical enclosures," *Progress In Electromagnetics Research*, Vol. 70, 225–246, 2007.
2. Anastassiu, H. T., J. L. Volakis, D. C. Ross, and D. Andersh, "Electromagnetic scattering from simple jet engine models," *IEEE Transactions on Antennas and Propagation*, Vol. 44, No. 3, 420–421, 1996.
3. Moffatt, D. L., C. Y. Lai, and T. Lee, "Time-domain electromagnetic scattering by open ended circular waveguide and related structure," *Wave Motion*, Vol. 6, No. 4, 363–387, 1984.
4. Galyamin, S. N., "Cherenkov wakefield radiation from an open end of a three-layer dielectric capillary," *arXiv preprint arXiv:2205.03986*, 2022.
5. Davis, A. M. J. and R. W. Scharstein, "Electromagnetic plane wave excitation of an open-ended, finite-length conducting cylinder," *Journal of Electromagnetic Waves and Applications*, Vol. 7, No. 2, 301–319, 1993.
6. Zhou, Z. and J. Huang, "Study of the radar cross-section of turbofan engine with biaxial multirotor based on dynamic scattering method," *Energies*, Vol. 13, No. 21, 5802, 2020.
7. Sun, X., "Influence evaluation of UAV inlet on electromagnetic scattering and time-frequency characteristics," *Journal of Physics: Conference Series*, Vol. 1971, No. 1, 012019, IOP Publishing, 2021.
8. Siouris, G. M., *Missile Guidance and Control Systems*, Springer-Verlag, New York, NY, USA, 2010.
9. Hussein, K. F. A., A. O. Helmy, and A. S. Mohra, "Radar pulse compression with optimized weighting window for SAR receivers," *Wireless Personal Communications*, Vol. 126, No. 1, 871–893, Sep. 2022.